Nanostructured Bacterial Cellulose–Poly(4-styrene sulfonic acid) Composite Membranes with High Storage Modulus and Protonic Conductivity

Tiago D. O. Gadim,[†] Andrea G. P. R. Figueiredo,[‡] Nataly C. Rosero-Navarro,[†] Carla Vilela,[‡] José A. F. Gamelas,[§] Ana Barros-Timmons,[‡] Carlos Pascoal Neto,[‡] Armando J. D. Silvestre,[‡] Carmen S. R. Freire,*,[‡] and Filipe M. L. Figueiredo*,[†]

[†]Department of Materials & Ceramic Engineering, CICECO, University of Aveiro, 3810-193 Aveiro, Portugal

[‡]Department of Chemistry, CICECO, University of Aveiro, 3810-193 Aveiro, Portugal

[§]Chemical Process Engineering and Forest Products Research Center, Chemical Engineering Department, University of Coimbra, Pólo II, R. Sílvio Lima, 3030-790 Coimbra, Portugal

S *Supporting Information*

ABSTRACT: The present study reports the development of a new generation of bio-based nanocomposite proton exchange membranes based on bacterial cellulose (BC) and poly(4-styrene sulfonic acid) (PSSA), produced by *in situ* free radical polymerization of sodium 4-styrenesulfonate using poly-(ethylene glycol) diacrylate (PEGDA) as cross-linker, followed by conversion of the ensuing polymer into the acidic form. The BC nanofibrilar network endows the composite membranes with excellent mechanical properties at least up to 140 °C, a temperature where either pure PSSA or Nafion are soft, as shown by dynamic mechanical analysis. The large concentration of sulfonic acid groups in PSSA is responsible for the high ionic exchange capacity of the composite membranes, reaching 2.25 mmol g^{-1} for a composite with 83 wt % PSSA/PEGDA. The through-plane protonic conductivity of the best membrane is in excess of 0.1 S cm^{-1} at 94 °C and 98% relative humidity (RH), decreasing to 0.042 S cm^{-1} at 60% RH. These values are comparable or even higher than those of ionomers such as Nafion or polyelectrolytes such as PSSA. This combination of electric and viscoelastic properties with low cost underlines the potential of these nanocomposites as a bio-based alternative to other polymer membranes for application in fuel cells, redox flow batteries, or other devices requiring functional proton conducting elements, such as sensors and actuators.

KEYWORDS: *bacterial cellulose, polystyrene sulfonic acid, nanostructured composite, protonic conductivity*
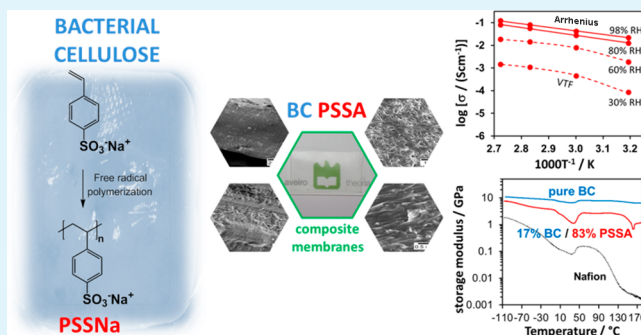
INTRODUCTION

The current concern with the environment, waste accumulation, and disposal, aggravated by the international geopolitical instability, is increasing to a point where sustainability, together with cost and functional characteristics, became a key issue for the development of novel materials, processes, and technologies. Energy storage and conversion are at the center of these concerns due to the inevitable depletion of fossil resources and climate change associated with CO_2 emissions. The hydrogen energy vector and fuel cell technologies, namely the polymer electrolyte membrane fuel cells (PEMFC), are key for the development of a new sustainable energy paradigm.[1] However, sustainability is still not a major concern of those involved in the research and development of fuel cell materials. The exception is the search for alternatives to the platinum catalyst, but in this particular context, sustainability is a synonym for rarity and prohibitive cost.[2]
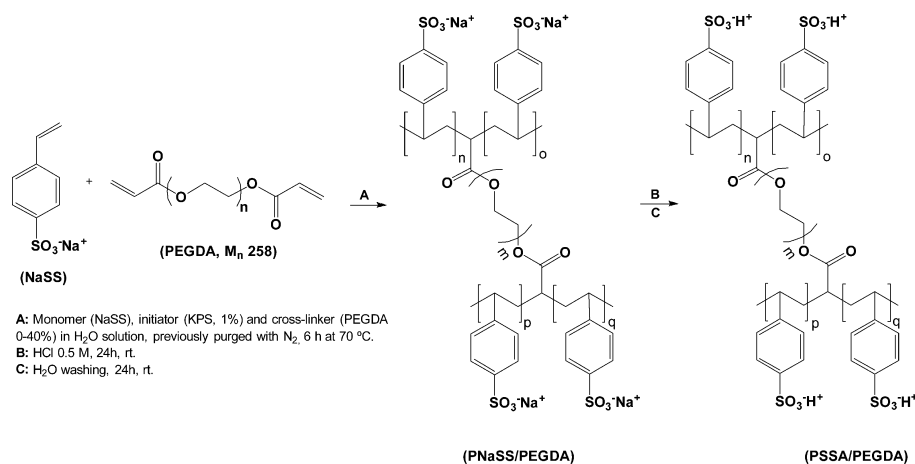
The polymer electrolyte has been (jointly with the catalyst) the PEMFC component deserving most of the R&D efforts due to the unsatisfactory performance of the state-of-the-art perfluorosulfonic acid (PFSA) membrane materials such as Nafion.[3,4] These membranes consist of an hydrophobic fluorocarbon backbone with side chains tipped by sulfonic acid groups, which when hydrated generate the hydrophilic domains where the proton exchange and transport take place.[5,6] The conductivity of this type of membranes is significantly decreased under low humidity or above 90 °C. The mechanical resistance is also diminished above 100 °C, whereas the hydrogen gas permeability and electro-osmotic drag of water should be desirably smaller.[5−7] The search for alternative

Scheme 1. Polymerization Scheme of NaSS into the PSSA Acidic Form with Cross-Linker PEGDA

A: Monomer (NaSS), initiator (KPS, 1%) and cross-linker (PEGDA 0-40%) in H_2O solution, previously purged with N_2, 6 h at 70 °C.
B: HCl 0.5 M, 24h, rt.
C: H_2O washing, 24h, rt.

materials has been exhaustive, from the development of new polymers to the modification of existing ones. Yet, most represent just incremental improvements.[8−14] This reflects the difficulty in finding a material meeting all the stringent requirements for application as a membrane separator in PEMFC, i.e., conductivity, adequate mechanical performance, gas tightness, and dimensional and chemical stability against strong acidic and oxidative conditions, and all in a compressed stack subjected to temperatures up to 100 °C (desirably higher than 120 °C) and to highly variable humidity conditions (from dry to saturation). It is thus not surprising that adding the "eco-friendly" requirement has not been a major concern in PEMFC research so far, with just a couple of known examples.

Chitosan is the most studied "green" material for fuel cell applications,[15] offering vast possibilities for chemical modification[16] and easily forming composites with other protonic conducting phases. However, the chemical and mechanical stability of these materials is clearly insufficient due to the well-known solubility of chitosan in diluted acidic aqueous solutions. Cellulose is the most abundant natural polymer and has been used in the form of carbon aerogels as a catalyst support,[17,18] and as membrane cross-linked with sulfosuccinic acid.[19] The conductivity of this membrane is reasonable (0.02 S cm^{-1} at room temperature), but the mechanical properties are more than one order of magnitude behind those of Nafion, probably due to the amorphous nature of the cross-linked structure.

Bacterial cellulose (BC) produced by some non-pathogenic bacteria is a highly pure and crystalline form of cellulose with a three-dimensional, cross-linked nano- and microfibrilar structure.[20] The excellent mechanical properties and biocompatibility of BC have generated considerable interest in this material for a variety of applications on the biomedical area[21−23] or as a composite reinforcement.[24−27]

Barbara Evans and co-workers were the first to notice the application of BC as a protonic conductor by demonstrating the anodic oxidation of H_2 via an acid displacement reaction and the concomitant electric current generation.[28] The current of this fuel cell, however, was very low (0.2 mA/0.48 V at room temperature) due to the intrinsic low conductivity of the electrolyte, a BC membrane treated in KCl. The idea was later recovered to produce platinum/BC catalyst layers assembled with a BC electrolyte modified with $H_3PW_{12}O_{40}·29H_2O$.[29] The power output of this fuel cell in an anhydrous H_2/O_2 gradient was less than 20 mW cm^{-2} at 55 mA cm^{-2} (at 40 °C), most likely due to the large ohmic drop in the electrolyte.

Unfortunately, this paper does not report any information on the protonic conductivity nor on the thermal and chemical stability of the materials.

To the best of our knowledge, only two systematic attempts to obtain highly conductive BC-based electrolytes have been reported so far. The first paper retrieves the example of polybenzimidazole/phosphoric acid composites[30] by doping the BC membranes with an anhydrous protonic conductor such as phosphoric or phytic acid.[31] As expected, the conductivity levels in anhydrous conditions may be high (>0.1 S cm^{-1}), but considering these excellent figures, the power output obtained under humidified H_2/O_2 gradients is rather low (<25 mW cm^{-2} at 60 mA cm^{-2}). The second paper reports the chemical modification of BC by a UV-induced graft polymerization of 2-acrylamido-2-methyl-1-propanesulfonic acid as a strategy to avoid acid leaching in contact with water.[32] Analogously to the PFSA membranes, the presence of water in the structure is fundamental to achieve the reported good levels of conductivity (~0.03 S cm^{-1} at room temperature).

All in all, less than five papers were published in the last 10 years exploring BC as a base component for proton exchange membranes, but all with fuel cell applications in mind and all reporting properties clearly behind Nafion.

We have recently presented a new type of renewable nanostructured composite electrolyte consisting of a BC network and a cross-linked poly(4-styrene sulfonic acid) (PSSA) polyelectrolyte (Scheme 1).[33] PSSA is a low-cost polyelectrolyte with high protonic conductivity[34,35] that can be easily processed using green chemistry methods. However, being a polyelectrolyte, PSSA is highly soluble in water, and hence, it must be anchored—usually by grafting—to other stable polymers such as poly(vinylidenefluoride)[36] or poly-(fluoroethylene-co-hexafluoropropylene),[37] or cross-linked with a bifunctional monomer to avoid leaching. Grafting to another polymer also improves the relatively poor mechanical properties of PSSA.[38] While its liability to oxidative decomposition limits the use in PEMFC to low temperature (<60 °C),[35,39] it is seen as a low-cost, green alternative to Nafion as the proton conducting component of ionic polymer metal composite actuators for biomedical applications[40] or sensors for toxic gases.[41] All these factors make PSSA an excellent candidate to demonstrate the potential of BC as a proton exchange membrane support. Here, we present the full details of the synthesis and characterization of these novel BC/PSSA nanocomposites, highlighting the relationships between

Table 1. List of the Prepared Membranes Including Composition, Sulfur Content, Ionic Exchange Capacity, and Water Uptake Capacity

Sample	nominal composition				measured properties		
	w_{NaSS}/w_{BC}	w_{PEGDA}/w_{NaSS}	$w_{PSSA/PEGDA}/w_{BC}$	w_{BC}/w_{total}	[S] mmol g$^{-1,a}$	[H$^+$] mmol g$^{-1,b}$	water uptake %
PSSA/PEGDA (1:0.4)	-	0.4	-	-	2.19 ± 0.01	-	-
BC^c	1	-	-	1	-	0	100
BC/PSSA/PEGDA (1:5:0)	5.8	0	0.40	0.71	0.11 ± 0.01	0.09	100
BC/PSSA/PEGDA (1:5:0.1)	5.8	0.1	0.88	0.53	0.76 ± 0.20	1.76	150
BC/PSSA/PEGDA (1:5:0.2)	4.4	0.2	1.29	0.44	1.83 ± 0.19	1.88	185
BC/PSSA/PEGDA (1:5:0.4)	4.4	0.4	4.74	0.17	2.36 ± 0.22	2.25	165

^{a}Average of at least 2 values obtained for different pieces of the same membrane. ^{b}Value obtained with the piece of the membrane used for the conductivity measurements. ^{c}Membrane treated in 0.5 M HCl solution, as all composites.
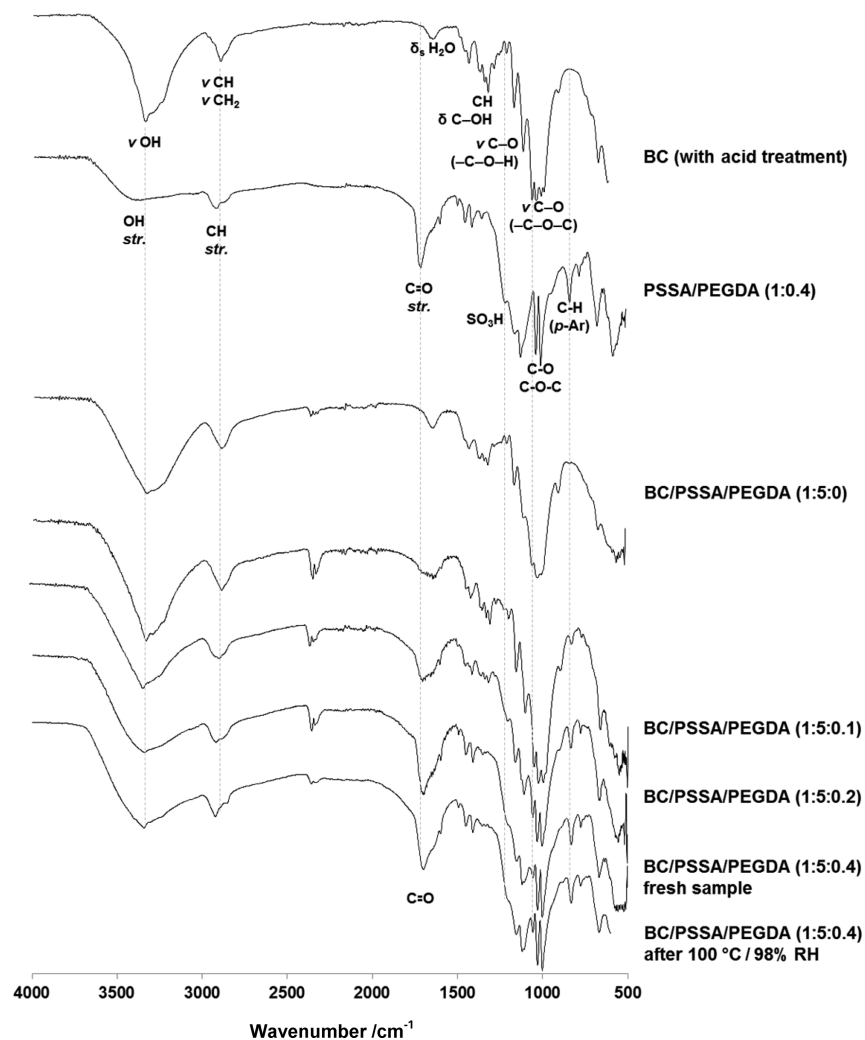
Figure 1. FTIR-ATR spectra of BC/PSSA/PEGDA nanocomposites (after washing and cation exchange), native BC (with acid treatment), and cross-linked polymer (PSSA/PEGDA).

structure, composition, viscoelastic behavior, and protonic conductivity.

RESULTS AND DISCUSSION

BC/PSSA nanocomposite membranes with variable concentrations of sulfonic acid groups were prepared by controlling the amount of poly(ethylene glycol) diacrylate (PEGDA) as cross-linker, according to the compositions listed in Table 1. The membranes were homogeneous and translucent after drying (Figure S1, Supporting Information). In this section, we

present and discuss a set of data obtained by various techniques providing a detailed characterization of the structure, microstructure, composition, thermo-chemical stability, and protonic conductivity of these nanocomposite membranes.

ATR-FTIR Spectroscopy. Figure 1 shows the FTIR spectra of native BC and BC/PSSA nanocomposite membranes with increasing contents of cross-linker (PEGDA). The cross-linker content is crucial to promote the polymer retention inside the BC tridimensional network, since after the washing and cation exchange procedure the spectrum of the nanocomposite

7866

dx.doi.org/10.1021/am501191t | ACS Appl. Mater. Interfaces 2014, 6, 7864−7875
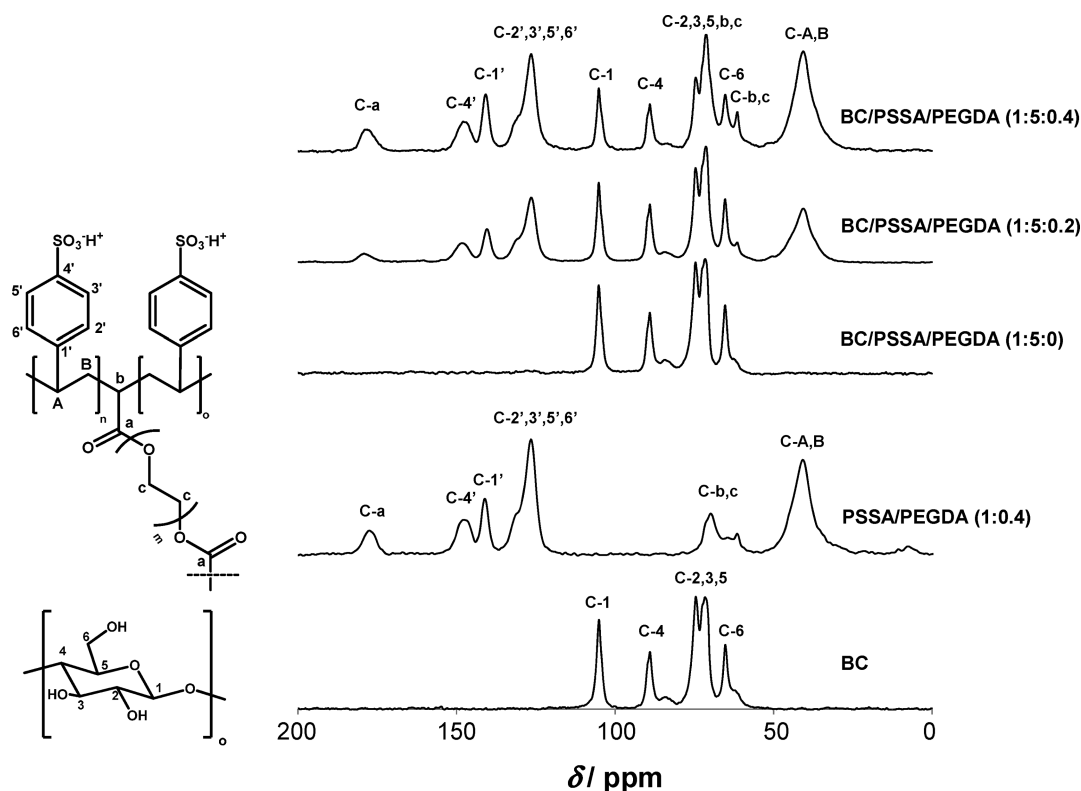
Figure 2. CPMAS ^{13}C NMR spectra of BC/PSSA/PEGDA nanocomposites (after washing and cation exchange), native BC (with acid treatment), and cross-linked polymer PSSA/PEGDA.

without cross-linker (BC/PSSA/PEGDA (1:5:0)) is very similar to that of pure BC. The typical bands of PSSA are still discernible in the spectrum of this composite, but with very low intensity, in agreement with the low sulfur content determined by CHNS elemental analysis (Table 1).

The success of the polymerization and retention of the cross-linked polymer inside BC was clearly confirmed by the appearance of the vibrations typical of PSSA (at 1597 cm^{-1} the ring skeletal vibration and at 860 cm^{-1} the aromatic out of plane C−H deformation in *para*-substituted rings), of sulfonic acid moieties (several absorptions in the range 1310−1060 cm^{-1}), and of one peak at around 1720 cm^{-1} assigned to the stretching of the carbonyl (C=O) group of the ester moiety of PEGDA. The vibrations at 3350 cm^{-1} (O−H stretching), 2930 cm^{-1} (C−H stretching), and 1060−920 cm^{-1} (stretching of C−O−C and C−O) are typically of both BC and cross-linked PSSA polymeric chains.

The proportional increment of the intensity of the vibrations assigned to the PSSA polymeric chains with increasing PEGDA content indicates that the retention of PSSA inside the BC network increases with the amount of cross-linker. The concomitant increment of the cross-linker content in the membranes is also evidenced by the increase of the intensity of the band due to the stretching vibration of PEGDA carbonyl group, at 1720 cm^{-1}. These FTIR results are in general agreement with the weight-gains ($w_{PSSA/PEGDA}/w_{BC}$) measured for each sample (Table 1).

Solid-State ^{13}C NMR Spectroscopy. Figure 2 displays the solid-state ^{13}C NMR spectra of the BC/PSSA/PEGDA nanocomposites, pure BC, and the PSSA cross-linked with 40% PEGDA. The spectra profile of the composite membranes is a perfect sum of the typical BC carbon resonances at δ 65.2 ppm (C-6), 71.4−74.3 ppm (C-2,3,5), 90.0 ppm (C-4) and

104.8 ppm (C-1)[42] with those of cross-linked PSSA at 40.8 ppm (C-A,B), 61.5 and 69.8 ppm (C-b,c), 126.5 ppm (C-2′,3′,5′,6′), 141.1 ppm (C-1′), 147.7 ppm (C-4′), and 177.5 ppm (C=O). The resonances attributed to PSSA are completely absent in the spectrum of the composite BC/PSSA/PEGDA (1:5:0), but their intensity increases regularly in the spectra obtained for the membranes with increasing fraction of PEGDA. These results again confirm the role of cross-linking in the retention of PSSA inside the BC network, and are in close agreement with the FTIR data and weight-gains. Finally, no clear evidence of deviations on the ^{13}C resonances was observed, suggesting that no complex interactions between BC and cross-linked PSSA were established.

Ion Exchange Capacity, Sulfur Content, and Water Uptake. The ion exchange capacity (IEC) is a direct measure of the content of sulfonic acid groups in the material and is, therefore, proportional to the amount of PSSA retained in the tridimensional network of BC. Table 1 shows that the IEC increases with increasing fraction of PEGDA, confirming that cross-linking increased the retention of PSSA in the host network of BC. High IEC values in excess of 1.5 mmol g^{-1} were obtained for these membranes, as expected for a polyelectrolyte such as PSSA present in large amounts in the composites.[34] Not surprisingly, these values are higher than those of commercial perfluorinated sulfonic acid ionomer membranes such as Nafion (~0.9 mmol g^{-1})[43] or Aquivion (~1.2 mmol g^{-1}).[44]

In general, the IEC for the composite membranes with high cross-linker content are in good agreement with the sulfur concentration ([S]) obtained by elemental analysis (Table 1). The deviation for the BC/PSSA/PEGDA (1:5:0.1) ([H$^+$] = 1.76 mmol g^{-1} vs [S] = 0.76 mmol g^{-1}) is indicative of some

7867

dx.doi.org/10.1021/am501191t | *ACS Appl. Mater. Interfaces* 2014, 6, 7864−7875

heterogeneity of the PSSA/PEGDA distribution within the BC for composites prepared using a lower amount of cross-linker.

As an additional confirmation of the effectiveness of the proposed cross-linking approach to imbed the polymer in the BC network, we note the similarity (within experimental error) between the sulfur content obtained for the cross-linked polymer PSSA/PEGDA (1:0.4) ([S] = 2.19 mmol g^{-1}) and for the corresponding BC nanocomposite BC/PSSA/PEGDA (1:5:0.4) ([S] = 2.36 mmol g^{-1}).

The dry BC membrane can absorb about its own weight of water (Table 1). The same water uptake capacity is observed for the BC/PSSA/PEGDA (1:5:0) membrane (without cross-linker), confirming the very low PSSA amount retained in this membrane. The addition of 10% PEGDA increases the water uptake to 150%, which further increases to 185% for 20% cross-linker, due to the presence of increasing amounts of highly hygroscopic sulfonic acid groups. Interestingly, doubling the PEGDA content to 40% has no obvious impact on the water uptake capacity, which is higher than that of the Nafion reference value (~50%), measured here under the same experimental conditions.

Parallel to the conductivity measurements, the thickness of control samples was monitored as a function of temperature and relative humidity (RH). The membranes at 94 °C/98% RH are 20 to 25% thicker than in the dry state. On the other hand, the expansion along the membrane plane was negligible, probably due to the highly anisotropic microstructure of these membranes. The apparent stabilization of the swelling behavior for higher PEGDA content also suggests that the cross-linking may be advantageous in controlling the volume changes upon hydration. Moreover, it should be noted that the anisotropic hydrolytic expansion of this kind of membranes may actually be controlled *in situ* by mechanical compression, such as in a fuel cell stack or other type of multilayered hetero-structures.

X-ray Diffraction. Figure 3 confirms the crystalline nature of BC in its pristine form and in the derived nanocomposite
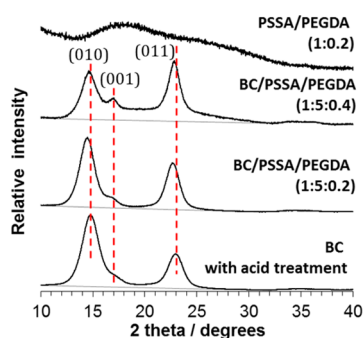
Figure 3. X-ray diffraction patterns of the BC nanocomposite membranes and of their individual components.

membranes, whereas the diffraction pattern of the cross-linked PSSA is typical of an amorphous material. The BC reflections can be indexed in the triclinic space group *P*1 of type Iα cellulose, and also in the monoclinic space group *P*2$_1$ of type Iβ cellulose.[45] Since type Iα is usually dominant in cellulose from bacterial origin,[45] we retain the *P*1 space group to index the patterns. The nanometric size of the crystalline domains originates fairly broad, overlapping peaks, and only the (010), (001), and (011) reflections are clearly distinguished at 2θ of approximately 14.9°, 16.3°, and 22.5°. These are the general features of XRD patterns of BC reported in the literature,

except the fact that quite often the (011) peak is sharper than the (010) and the (001).[46,47] The (011) plane corresponds to the distance between sheets connected by weak electrostatic interactions (Figure S2, Supporting information),[45] which might be destroyed by the aqueous HCl treatment necessary to protonate the composite membranes (also applied to the pure BC). The intra-sheet structure, which includes planes (010) and (001), containing much stronger covalent bonds along the cellulose chains and on the hydrogen bond network, seems to be affected by the presence of the cross-linked PSSA. Indeed, the intensity of (010) reflection relatively to (011) decreases with increasing amount of PSSA/PEGDA, which is indicative of smaller volume of planes with high density of O—H···O bonds. Moreover, the difference between the intensity of the (010) and (011) reflections decreases with increasing PSSA content, being accompanied by a slight decrease of the unit cell volume, apparent in the shift of the peak position to lower angles. These are features typically found in patterns of samples with higher content of type Iβ cellulose.[46,47] The Iα $\Rightarrow$ Iβ transition involves breaking hydrogen bonds allowing the Iα chains to rotate and adopt a stable and compact structural arrangement of the type Iβ, a process normally induced by temperature above 200 °C.[45,48] The strong sulfonic acid groups in the BC/PSSA/PEGDA composites seem to disturb the hydrogen bonds of cellulose leading to similar structural rearrangements at lower temperatures.

Interestingly, there is no noticeable decrease of the integral breadth of the peaks that could indicate a decrease of the overall crystallinity of the cellulosic fraction of the composite. Nevertheless, one can observe in the BC/PSSA/PEGDA (1:5:0.4) pattern a clear deviation of the base line for an intermediate 2θ range between the (001) peak and 2θ = 30° that may be ascribed to the presence of disordered cellulose domains.[49] It is perhaps important to notice that this 2θ range also coincides with the amorphous-like feature depicted by the pattern of cross-linked PSSA[50] (top of Figure 3, similar to that in ref 51), which may thus also explain the increased counts in the BC/PSSA/PEGDA (1:5:0.4) pattern.

SEM. Selected SEM micrographs of the surface and cross-section of BC/PSSA/PEGDA (1:5:0.1) and BC/PSSA/PEGDA (1:5:0.4) membranes are shown in Figure 4 as examples of the typical microstructure of the composite membranes. The observation of the characteristic tridimensional nanofibrilar network and lamellar microstructure of BC (Figure S3, Supporting Information) indicates that those were not destroyed or affected during the various steps of the nanocomposites preparation. It is also apparent that the network of the layered cellulose nanofibrils is impregnated with the cross-linked PSSA/PEGDA matrix and that the amount of PSSA/PEGDA retained increases with increasing the cross-linker content. This is better illustrated by views of the membrane cross-section, where the lamellar spaces are progressively filled with the polymer as the PEGDA content increases.

This highly anisotropic microstructure is responsible for several properties of the nanocomposites. On the one hand, the alignment of the BC mats parallel to the plane of the membrane should promote a desirable high compressive strength suitable to easily sustain the compressive forces of, e.g., a fuel cell stack. This is also expected to minimize the formation of cracks resulting from the hydrolytic expansion of the membrane plane associated with the hydration/dehydration cycles. On the other hand, the BC mats represent resistive layers to the protonic
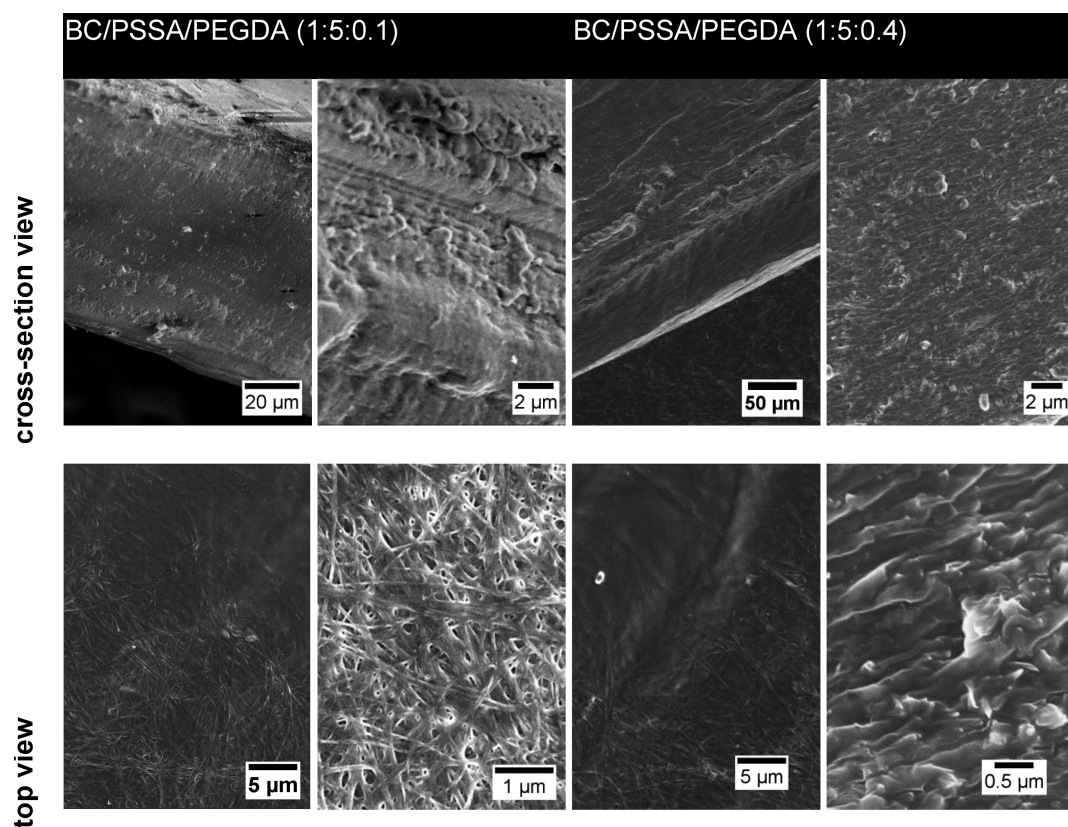
Figure 4. SEM micrographs of the nanocomposite membranes BC/PSSA/PEGDA (1:5:0.1) and BC/PSSA/PEGDA (1:5:0.4).

transport across the membrane plane. In this regard, the apparently homogeneous distribution of the PSSA through the entire membrane thickness is reassuring that electrical percolation can be achieved.

Thermogravimetric Analysis. The thermogravimetric analysis (TGA) of BC/PSSA/PEGDA nanocomposite membranes was carried out to evaluate their thermal stability and degradation profile (Figure 5). Reference samples of BC and PSSA/PEGDA (1:0.4) were also analyzed for comparison purposes. The acid-treated BC shows a weight-loss profile typical of cellulosic substrates, with initial and maximum decomposition temperatures at around 249 and 313 °C, respectively. These values are slightly lower than those of native bacterial cellulose (around 270 and 350 °C, respectively[52]), probably due to the applied acid treatment,[53,54] analogous to that used to neutralize the sulfonate groups in the composite membranes. In turn, the PSSA/PEGDA (1:0.4) reference starts to decompose at ~170 °C, well before pure BC, but the main weight-loss peak occurs almost at the same temperature (306 °C) as for BC (313 °C). The thermogram of the BC/PSSA/PEGDA (1:5:0) prepared without cross-linker is similar to that of the BC after the acid treatment, with initial decomposition at 190 °C and a maximum around 295 °C, in close agreement with the low PSSA content suggested by FTIR, NMR, and CHNS elemental analyses. The thermograms of the composite membranes show a clear weight-loss around 100 °C due to the release of absorbed water that increases with increasing fraction of cross-linker, reflecting the key role of the sulfonated polymer in the hydration capacity of these nanocomposites. These plots also reveal that the decomposition of membranes prepared using 10%, 20%, and 40% PEGDA show three or four thermal degradation steps starting at 140−190 °C with the correspond-
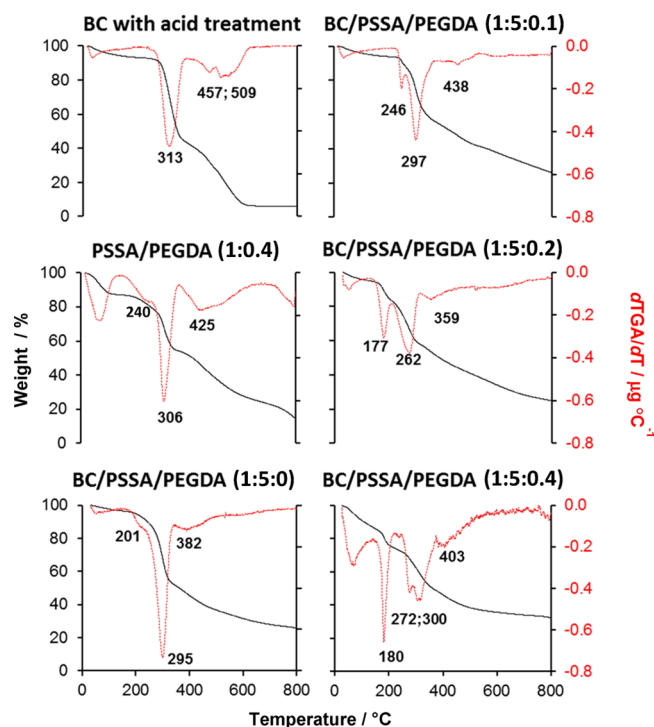

Figure 5. Thermograms and the corresponding derivative, obtained under N₂ atmosphere, of BC after the acid treatment, PSSA/PEGDA (1:0.4) and BC/PSSA/PEGDA composite membranes (0 to 40% cross-linker content).

ing maximum rates in the differential curves observed at 177−438 °C.

The distinct decomposition patterns of the composites when compared with the reference samples (BC and PSSA/PEGDA (1:0.4)) suggest the thermal activation of a chemical interaction between the BC and the PSSA/PEGDA leading to the membrane degradation. Nevertheless, the membranes are thermally stable up to approximately 140 °C.

Dynamic Mechanical Analysis. Figure 6A compares the storage modulus (E') of the BC/PSSA/PEGDA (1:5:0.4)
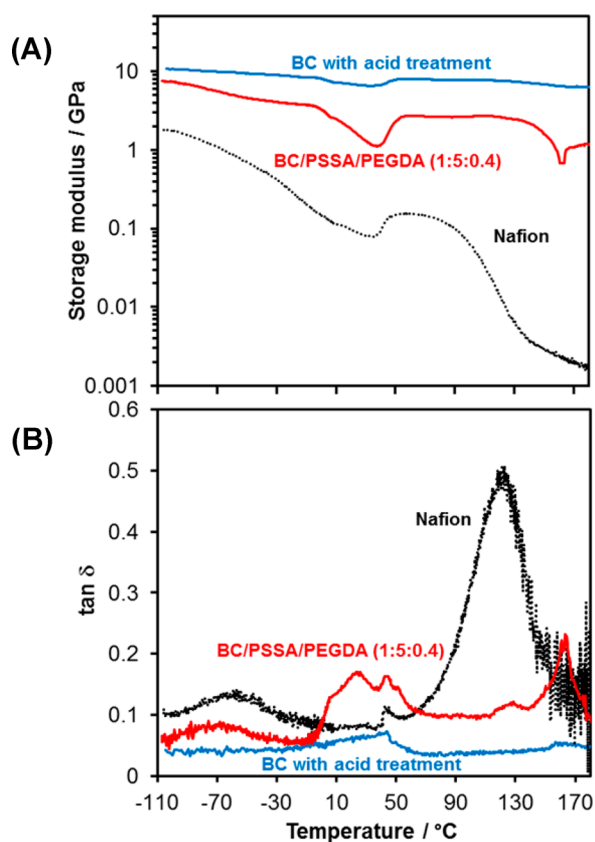
Figure 6. DMA data showing the comparison of the (A) storage modulus and (B) loss tangent of the BC/PSSA/PEGDA (1:5:0.4) nanocomposite membrane, BC after the acid treatment, and a plain Nafion membrane obtained in tension mode.

nanocomposite with pure BC and Nafion. The three samples display E' minima at nearly 0 °C. This is attributed to the plasticizing effect of water. Increasing the chamber temperature above room temperature lowers the RH and the samples loose water, recovering the elastic properties. The effect of this sudden dehydration is less pronounced for pure BC due to its highly crystalline and rigid network of nanofibrils. However, the analysis of the results has to take into consideration that the DMA chamber is not equipped with a controlled humidity system. For that reason, the reference Nafion membrane (extensively reported in the literature)[6,7] was studied under the same experimental conditions.

Apart from the particular relaxation around 0 °C, the viscoelastic behavior of BC is quite stable up to at least 170 °C, with E' decreasing slightly from 10 GPa at −100 °C to 6.4 GPa at 170 °C. These values are very similar to those measured for a pristine BC membrane (~10 GPa at 170 °C),[42] indicating that the acid treatment has little or no effect on the viscoelastic behavior of the material. Worth noting is also the fact that the E' of BC is more than one order of magnitude higher than that

of Nafion. Moreover, it remains almost unaffected by temperature and RH, whereas the storage modulus of Nafion strongly decreases above 70 °C, as amply documented.[6−8]

The excellent mechanical behavior of the pure BC membrane is reflected on the BC/PSSA/PEGDA composite, both on the magnitude of E' and on the thermo-mechanical stability. Indeed, for this composite E' is 2.65 GPa at 75 °C (i.e., at least 20 times higher than that of Nafion) and remains constant from 60 to ∼140 °C. However, the drop of E' between −10 and 60 °C is more pronounced than that observed for BC, in agreement with the higher water uptake capacity and the lower BC fraction of the composite. Finally, the additional relaxation at ∼160 °C indicates the onset of major structural changes in BC/PSSA/PEGDA associated with the thermal degradation.

The loss tangent data (tan δ) presented in Figure 6B confirm the temperature dependence of the storage modulus but provide a more exact indication of the transition temperatures. The main features reported in the literature for Nafion and for BC are detected here as well.[6,7,42] As regards the BC/PSSA/ PEGDA membranes, two small tan δ peaks at −70 and at 130 °C can be detected, which are not observed for BC, as well as two overlapping peaks between −10 and 60 °C, all attributed to the PSSA/PEGDA fraction. A direct comparison between BC and PSSA/PEGDA (1:0.4) could not be made as adequate PSSA/PEGDA films could not be prepared. In view of that, the behavior of pieces of PSSA/PEGDA (1:0.4) was compared with that of BC/PSSA/PEGDA (1:5:0.4) using the DMA material pocket accessory (Figure 7). The data for both samples show a
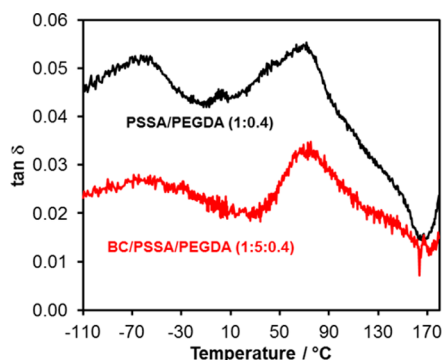
Figure 7. Loss tangent collected using the material pocket system for cross-linked PSSA/PEGDA and corresponding BC nanocomposite.

low temperature relaxation at around −70 °C already observed in Figure 6B. Additionally, a broad peak at ∼75 °C can also be detected for PSSA/PEGDA (1:0.4) suggesting an overlapping of distinct relaxations. A similar trend is observed for the composite membrane analyzed in the material pocket accessory though the second peak appears at a slightly lower temperature (70 °C). The clear attribution of the relaxations detected around −70 and 70 °C is not possible as many factors are involved. The discrepancy in the temperatures at which relaxations are detected in the composite membrane analyzed under the tension mode and when using the material pocket accessory may be associated with a variety of factors: (i) the fact that in the first case, macromolecules are under strain and in the latter only thermal effects are being assessed, (ii) the sample preparation procedure is not exactly the same, and, as mentioned earlier, (iii) the dimensions of the composite membrane measured under strain may be altered during the
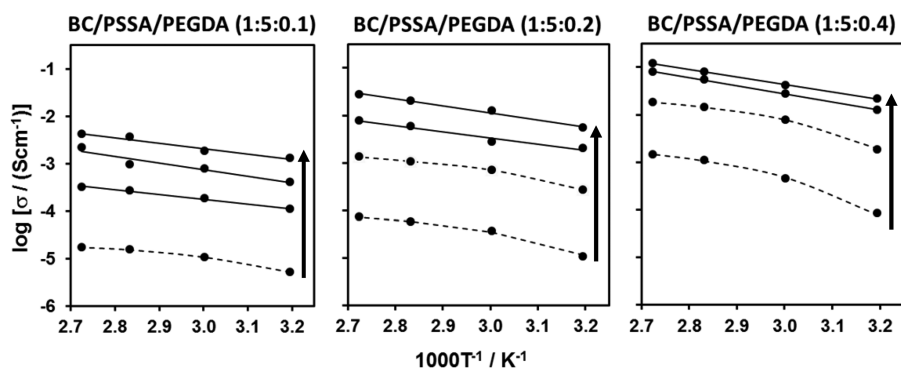
Figure 8. Arrhenius plots of the total conductivty of nanocomposite membranes with variable content of cross-linker measured at RH of 30%, 60%, 80% and 98% (increasing in the direction of the arrows). The straight lines are linear fits to the Arrhenius model, whereas the dashed curves are fits to the VTF equation (relevant fitting parameters shown in Table 2).

Table 2. Fitting Parameters of the Conductivity Data (Figure 8) to the Arrhenius (eq 1) or the VTF (eq 2) Equations[a]

| | relative humidity | | | |
sample	30%	60%	80%	98%
BC/PSSA/PEGDA	$T_0 = 3$	$E_a = 19$	$E_a = 28$	$E_a = 22$
(1:5:0.1)	$A = 8.12 \times 10^{-4}$			
	$B = 0.69$			
BC/PSSA/PEGDA	$T_0 = 4$	$T_0 = 3$	$E_a = 28$	$E_a = 31$
(1:5:0.2)	$A = 0.01$	$A = 0.09$		
	$B = 1.00$	$B = 1.10$		
BC/PSSA/PEGDA	$T_0 = 7$	$T_0 = 7$	$E_a = 33$	$E_a = 30$
(1:5:0.4)	$A = 0.18$	$A = 1.46$		
	$B = 1.37$	$B = 1.06$		

[a]E_a in kJ mol^{-1}, T_0 in °C, A in S cm^{-1} K$^{1/2}$ and B in kJ mol^{-1}.

analyses as a result of changes of the RH. Finally, in agreement with what was observed by TGA, above 140 °C the material decomposes.

Protonic Conductivity. Figure 8 shows Arrhenius plots of the conductivity of the BC/PSSA/PEGDA composite membranes measured under variable RH. It can be seen that the conductivity increases orders of magnitude with increasing PEGDA content for the entire range of temperature and RH, in a direct correlation with the IEC of each sample (Table 1). The conductivity of the best composite membrane is in excess of 0.1 S cm^{-1} at 94 °C/98% RH, decreasing to 0.042 S cm^{-1} at 60% RH. These values are amongst the highest reported for proton exchange membrane materials, being comparable or higher than data typically found in the literature for Nafion,[55−58] and other PSSA-based materials.[36,37,59−61]

For comparison, it is interesting to note that the conductivity of the pure BC membrane at 94 °C and 30% RH is 6 orders of magnitude lower than that for BC/PSSA/PEGDA (1:5:0.4), whereas the difference is strongly reduced to 3 orders of magnitude at 98% RH (data for BC in Figure S6, Supporting Information). While the pure BC membrane has some ability to retain water even at temperatures close to 100 °C and in conditions close to saturation, this comparison demonstrates that the high conductivity of the composite is mostly due to the sulfonic acid groups of PSSA.

The simple visual inspection of Figure 8 shows that the temperature dependence of the conductivity (σ) of the three composites at the highest RH follows the usual Arrhenius behavior (solid lines), according to eq 1:

$$\sigma = \sigma_0 \exp[-E_a(RT)^{-1}] \qquad (1)$$

where σ_0 is a pre-exponential term, E_a is the activation energy for proton transport, R is the gas constant, and T is the absolute temperature. All E_a values are close to 30 kJ mol^{-1} (Table 2). Nafion has lower E_a (10−20 kJ mol^{-1}) under similar conditions, in agreement with the literature.[5,62,63] Even without any information on the morphology of the PSSA/PEGDA, which might have great impact on the conductivity,[34] one may argue that the higher E_a of the composite membranes may be explained by the stronger proton attraction exerted by the much higher concentration of sulfonic acid groups in PSSA/PEGDA (>1.7 mmol g^{-1}) than in Nafion (0.9 mmol g^{-1}).

The deviation from the Arrhenius behavior for low RH is obvious in Figure 8, showing a curvature that recalls the Vogel−Tamman−Fulcher (VTF) equation

$$\sigma = A \exp[-B(T - T_0)^{-1}] \qquad (2)$$

where A is a pre-exponential term related to the charge carrier density that depends on temperature according to $A = \sigma_0 T^{-1/2}$, B is an activation energy term related to the migration of the smallest segmented polymer chain, and T_0 is an equilibrium temperature (also known as the Vogel temperature), below which the migration vanishes and only vibrations occur. Good fits to the VTF equation (dashed lines in Figure 8) were obtained for the three membranes at 30% and 60% RH, except for the BC/PSSA/PEGDA (1:5:0.1) at 60% RH (although a small curvature is still perceptible). In general, the fitting parameters (Table 2) are close to the results obtained for a variety of amorphous protonic conductors (including polymers, organic-inorganic hybrids and composites of phosphoric acid with a polymer[64−66]), with the expected exception of T_0, since it is closely related to the glass transition assisting proton

migration. Thus, one should be able to correlate T_0 with the viscoelastic behavior of the membranes.

Indeed, a good agreement with the DMA results is also found when the general relation between the Vogel and the glass transition temperature expressed by eq 3[67] is applied to data of BC/PSSA/PEGDA (1:5:0.4).

$$T_0 = 1.05T_g - 77 \qquad (T_0 \text{ and } T_g \text{ in Kelvin}) \qquad (3)$$

The T_0 fitted to the data obtained for this sample (7 °C) is in remarkable agreement with the estimate (10 °C) of eq 3 using the tan δ peak temperature determined by DMA (70 °C, Figure 7). This clearly suggests that the segmented migration (though restricted) of the same synthetic moieties is responsible for the observed viscoelastic (assessed by DMA) and electric ionic (by impedance spectroscopy) relaxations. Even in the sample prepared using 20% of cross-linker the similarity is still significant. The fact that the activation energy term is approximately 1 kJ mol^{-1} in all studied cases where the VTF equation holds, suggests (within the frame of the Adam–Gibbs theory) that the elemental size of the migrating entities is the same. On the contrary, the pre-exponential term, which is related to the concentration of the charge carriers, increases by almost one order of magnitude with increasing RH from 30 to 60%, regardless of the concentration of sulfonic acid groups in the composite, in agreement with the expected higher hydration of the material at higher RH. All these observations demonstrate the role of water as a plasticizer of the cross-linked PSSA structure, which when is partly hydrated (as expected for the low RH) is sufficiently mobile to assist proton migration across the sulfonated polymeric chains. Increasing the RH increases the water content in the membrane to such a level that the conductivity is then dominated by the proton structural diffusion in the water layers and less influenced by the sulfonic acid groups.

Finally, it is important to notice that the BC/PSSA/PEGDA membranes retained the mechanical integrity after the electrical measurements at 100 °C with 98% RH in the presence of the metallic silver electrodes. Moreover, the FTIR analysis of these samples did not show signs of chemical modification (bottom spectrum in Figure 1). This is a particularly relevant result considering the application of this type of membranes in a PEMFC, where the strong oxidizing conditions resulting from the combination of high humidity and high acid concentration, further catalyzed by the electrode platinum catalyst nanoparticles, are so demanding that the PSSA is known not to resist above 100 °C.[39]

CONCLUSIONS

In conclusion, novel nanocomposites consisting of cross-linked PSSA supported on a bacterial cellulose tridimensional nanofribilar network were prepared and characterized as proton exchange membranes. Mechanically and thermally stable nanocomposites with up to 83 wt % PSSA/PEGDA can be easily obtained with no evidence for strong chemical interaction between the composite components.

Due to the polyelectrolyte nature of PSSA, ionic exchange capacities in excess of $[H^+] = 2$ mmol g^{-1} can be obtained for about 80 wt % PSSA/PEGDA, whereas the membrane swelling due to water uptake is limited by the rigid cellulose network. The cellulose matrix is also responsible for the stable viscoelastic behavior of the nanocomposite membranes, yielding storage modulus values more than one order of

magnitude higher than for Nafion, until the onset of thermal degradation at ~140 °C.

As expected, the protonic conductivity of the composite membranes increases with increasing concentration of sulfonic acid groups, and again exceeds the performance of the state-of-the-art PFSA-type membranes. As for the latter type of materials, the temperature dependence of the conductivity displays an Arrhenius-type behavior but only for high humidity. The Arrhenius-type law fails for low relative humidity (60% and lower), and the data is better fitted by a VTF-type equation assuming a proton transport mechanism assisted by the segmental motion of cross-linked PSSA chains, in agreement with DMA data.

In addition to this competitive combination of electric and viscoelastic properties, these new nanocomposites also offer a potential low cost advantage, and represent the first bio-based alternative to PFSA-type materials for fuel cells and other devices where proton conductors are key functional elements, such as sensors and actuators for biomedical applications. Current work is focused on the development of membrane-electrode assemblies based on the BC-based nanocomposite membranes, and their testing in a hydrogen/air single cell configuration to assess the long-term cell performance and how it is affected by the operation conditions, namely the relative humidity and temperature.

MATERIALS AND METHODS

Membrane Preparation. *Chemicals.* Sodium 4-styrenesulfonate (NaSS, ≥90%, Aldrich), potassium persulfate (KPS, 98%, Panreac), poly(ethylene glycol) diacrylate (PEGDA, M_n 258, Aldrich), Nafion (M_n 1100, Aldrich). All reagents were used without previous purification.

BC Membranes. Bacterial cellulose (BC), a tridimensional network of nano and microfibrils with 10–200 nm width, in the form of wet membranes was produced at our laboratory using the *Gluconoaceto-bacter sacchari* bacterial strain[68] and following established culture procedures[69] detailed in Supporting Information.

BC-PSSA Nanocomposite Membranes. Wet BC membranes (4 × 4 cm^2, 0.8 cm thickness, 99% humidity) were weighted, and 60% of their water content (~5 mL) was drained by hand-pressing between two acrylic plates at room temperature, before being placed into Erlenmeyers with septa and purged with nitrogen. Simultaneously, 5 mL of aqueous solutions of NaSS with a concentration determined by the dry mass of the corresponding BC membrane (BC:NaSS mass ratio of 1:5), KPS (1.2%, w_{KPS}/w_{NaSS}), and variable amounts of PEGDA (0, 10, 20, and 40% w_{PEGDA}/w_{NASS}) was prepared in an ice bath and purged with nitrogen for 30 min and then allowed to reach room temperature. Each solution was transferred with a syringe into an Erlenmeyer containing a drained BC sample. The membranes were left to stand for approximately 1 h at room temperature (25 °C) until the complete absorption/incorporation of the solution and then left for 6 h at 70 °C in N_2 atmosphere. Finally, the septa were pulled off, and the solution cooled naturally overnight. The modified BC membranes were washed several times in distilled water volumes of 100 mL for 30 min until the conductance of the supernatant was equal to, or lower than, 20 μS cm^{-1}. The washed membranes were dried at 40 °C for 5–12 h and analyzed by FTIR-ATR (as described elsewhere in this section) to confirm the success of the polymerization. All experiments were made in quadruplicate. Finally, the membranes were converted into the acid form by ionic exchanging with an aqueous solution of 0.5 M HCl (100 mL) for 24 h at room temperature. The acidic membranes were again washed with distilled water following the above mentioned protocol, dried at 40 °C, and kept in a desiccator until further use. The membranes can be obtained with thicknesses ranging from 50 to 300 μm, as measured by a micrometer and further confirmed by SEM. One sample of each nanocomposite (and also pure BC) was also frozen in liquid nitrogen, freeze-dried for 3 days in a

Virtis Benchtop K freeze-drier under a vacuum pressure of 4 Pa, and weighed. The PSSA/PEGDA and BC percent composition of the nanocomposites (Table 1) were estimated by difference to the original BC weight.

Cross-Linked PSSA. Reference samples of PSSA cross-linked with PEGDA, corresponding to 40% w_{PEGDA}/w_{NaSS} were prepared using the same procedure described for the preparation of nanocomposite membranes, obviously omitting the impregnation step.

Nafion Membranes. For comparison purposes, a Nafion membrane was also prepared by casting, as described in the Supporting Information.

Characterization. *Structure and Microstructure.* All ensuing membranes, dried at 40 °C, were characterized using FTIR, ^{13}C NMR, X-ray diffraction (XRD), and scanning electron microscopy (SEM).

The FTIR spectra were taken with a PerkinElmer FT-IR System Spectrum BX spectrophotometer equipped with a single horizontal Golden Gate ATR cell, over the range of 600−4000 cm^{-1} at a resolution of 4 cm^{-1} averaged over 32 scans.

CPMAS ^{13}C NMR spectra were recorded on a Bruker Avance III 400 spectrometer operating at a B0 field of 9.4 T using 9 kHz MAS with proton 90° pulse of 3 μs, time between scans of 3 s, and a contact time of 2000 μs. ^{13}C chemical shifts were referenced with respect to glycine (C=O at 176.03 ppm).

SEM micrographs of the film surfaces and cross-sections were obtained on a HR-FESEM SU-70 Hitachi equipment with a EDS Bruker QUANTAX 400 detector operating at 4 kV. The samples were previously coated with a carbon film.

The XRD analysis was carried out on a Phillips X'pert MPD diffractometer using Cu Kα radiation (λ = 1.541 Å) with a scan rate of 0.05° s^{-1} (in 2θ scale). The patterns were collected in reflection mode with the membranes placed on a Si wafer with negligible background signal to provide mechanical support avoiding the bending of the membrane.

Elemental Analysis. Elemental analysis (CHNS) was carried out in a LecoTruspec2061 series 4555 equipment, using a sample size of up to 10 mg, a combustion furnace temperature of 1075 °C, and an afterburner temperature of 850 °C. All samples were crushed, frozen in liquid nitrogen, and then lyophilized for 3 days before the analysis of a minimum of 2 replicas per sample.

Thermogravimetric Analysis. TGA essays were carried out with a Shimadzu TGA 50 analyzer equipped with a platinum cell. Samples were heated at a constant rate of 10 °C min^{-1} from room temperature up to 800 °C under a nitrogen flow of 20 mL min^{-1}. The thermal decomposition temperature was taken as the onset of significant (~0.5%) weight-loss, after the initial evaporation of moisture.

Water Uptake. The water uptake (W) is expressed as the difference in weight of the membranes in the wet (w_w) and dry states (w_d) normalized to the dry weight

$$W(\text{wt \%}) = (w_w - w_d)w_d^{-1} \times 100 \qquad (4)$$

The w_d was obtained after drying the membranes at 60 °C (less than 1% RH) for several hours until no mass changes could be measured. After an immersion step in de-ionized water at room temperature for 24 h, the membranes were taken out, and w_w was measured immediately after wiping the surface with a filter paper.

Ion Exchange Capacity. Ion exchange capacity (IEC) measurements were performed by soaking the membranes in a aqueous 0.1 M NaCl for 24 h, followed by titration with 0.005 or 0.025 M aqueous NaOH solutions for membranes with low cross-linker contents (≤10%) or higher cross-linker contents (≥20%), respectively, according to

$$\text{IEC (mmol g}^{-1}) = (V_{NaOH} \times M_{NaOH})w_d^{-1} \qquad (5)$$

where V_{NaOH} is the volume (in mL) of the NaOH solution corresponding to the equivalence point and M_{NaOH} is the molar concentration of this solution.

Dynamic Mechanical Analysis. The DMA curves of rectangular pieces of membrane with 30 × 5 mm^2 were obtained on a Tritec 2000 DMA (Triton Technologies) operating in tension mode (single strain)

at 1 Hz and with 0.005 mm displacement. Smaller pieces with approximately 5 × 5 mm^2 were also analyzed using the material pocket system, in this case with a displacement of 0.020 mm. In both types of measurements, the temperature was sweep from -100 to 170 °C with a constant heating rate of 2 °C min^{-1}. Before the measurements, the materials were kept for 72 h in a conditioning cabinet at 30 °C/50% RH.

Protonic Conductivity. The through-plane protonic conductivity (σ) of the membranes was determined by electrochemical impedance spectroscopy (Agilent 2980A LCR meter) under variable temperature (40−100 °C) and relative humidity (20% to 98%) conditions in a climatic chamber (ACS Discovery DY110). Silver electrodes (Agar Scientific) were applied on both sides of the membrane, which was then placed between two carbon cloth gas diffusion layers and graphite plates with gas channels. The current was collected on top of both plates with platinum foils and connected to the LCR meter by platinum wires and co-axial cables using a pseudo 4-electrodes configuration. The impedance spectra (examples show in Figure S5, Supporting Information) were recorded between 20 Hz and 2 × 10^6 Hz with test signal amplitude of 100 mV, in some cases also with 500 mV (Figure S6, Supporting Information), and analyzed with the ZView software (Version 2.6b, Scribner Associates) in order to assess the ohmic resistance (R) of the membrane (details given in Supporting Information). The conductivity was then calculated using $\sigma = L(RA)^{-1}$, where L is the thickness of the dry membrane and A is the surface area of the electrodes.

■ ASSOCIATED CONTENT

Ⓢ Supporting Information
Additional information on the structure, the morphology/ microstructure and the protonic conductivity of pure bacterial cellulose membrane; obtained impedance spectra with interpretations; preparation of Nafion membranes. This material is available free of charge via the Internet at http:// pubs.acs.org.

■ AUTHOR INFORMATION

Corresponding Authors
*E-mail: cfreire@ua.pt.
*E-mail: lebre@ua.pt.

Notes
The authors declare no competing financial interest.

■ ACKNOWLEDGMENTS

■ REFERENCES

(1) Council of the European Union, *Council Regulation Setting Up the Fuel Cells and Hydrogen Joint Undertaking Multi-Annual Implementation Plan 2008−2013*, 8541/08, 2008.

(2) Sealy, C. The Problem with Platinum. *Mater. Today* **2008**, *11*, 65−68.

(3) Spendelow, J. S.; Papageorgopoulos, D.C. Progress in PEMFC MEA Component R&D at the DOE Fuel Cell Technologies Program. *Fuel Cells* **2011**, *11*, 775−786.

(4) Hoogers, G. In *Fuel Cell Technology Handbook*; Hoogers, G., Ed.; CRC Press: Boca Raton, FL, 2003; Chapter 4, pp 4-1−4-17.

(5) Kreuer, K. D.; Paddison, S. J.; Spohr, E.; Schuster, M. Transport in Proton Conductors for Fuel-Cell Applications: Simulations, Elementary Reactions, and Phenomenology. *Chem. Rev.* **2004**, *104*, 4637−4678.

(6) Mauritz, K. A.; Moore, R. B. State of Understanding of Nafion. *Chem. Rev.* **2004**, *104*, 4535−4586.

(7) Kreuer, K. D. The Role of Internal Pressure for the Hydration and Transport Properties of Ionomers and Polyelectrolytes. *Solid State Ionics* **2013**, *252*, 93−101.

(8) Young, S. K.; Mauritz, K. A. Dynamic Mechanical Analyses of Nafion®/Organically Modified Silicate Nanocomposites. *J. Polym. Sci. B: Polym. Phys.* **2001**, *39*, 1282−1295.

(9) Hogarth, W. H. J.; Diniz da Costa, J. C.; Lu, G. Q. Solid Acid Membranes for High Temperature (>140 °C) Proton Exchange Membrane Fuel Cells. *J. Power Sources* **2005**, *142*, 223−237.

(10) Zhang, J.; Xie, Z.; Zhang, J.; Tang, Y.; Song, C.; Navessin, T.; Shi, Z.; Song, D.; Wang, H.; Wilkinson, D. P.; Liu, Z. S.; Holdcroft, S. High Temperature PEM Fuel Cells. *J. Power Sources* **2006**, *160*, 872−891.

(11) Li, Q.; Jensen, J. O.; Savinell, R. F.; Bjerrum, N. J. High Temperature Proton Exchange Membranes Based on Polybenzimidazoles for Fuel Cells. *Prog. Polym. Sci.* **2009**, *34*, 449−477.

(12) Mustarelli, P.; Carollo, A.; Grandi, S.; Quartarone, E.; Tomasi, C.; Leonardi, S.; Magistris, A. Composite Proton-Conducting Membranes for PEMFCs. *Fuel Cells* **2007**, *7*, 441−446.

(13) Titvinidze, G.; Kreuer, K.-D.; Schuster, M.; de Araujo, C. C.; Melchior, J. P.; Meyer, W. H. Proton Conducting Phase-Separated Multiblock Copolymers with Sulfonated Poly(phenylene sulfone) Blocks for Electrochemical Applications: Preparation, Morphology, Hydration Behavior, and Transport. *Adv. Funct. Mater.* **2012**, *22*, 4456−4470.

(14) Subianto, S.; Pica, M.; Casciola, M.; Cojocaru, P.; Merlo, L.; Hards, G.; Jones, D. J. Physical and Chemical Modification Routes Leading to Improved Mechanical Properties of Perfluorosulfonic Acid Membranes for PEM Fuel Cells. *J. Power Sources* **2013**, *233*, 216−230.

(15) Ma, J.; Sahai, Y. Chitosan Biopolymer for Fuel Cell Applications. *Carbohydr. Polym.* **2013**, *92*, 955−975.

(16) Harish Prashanth, K. V.; Tharanathan, R. N. Chitin/Chitosan: Modifications and their Unlimited Application Potential—an Overview. *Trends Food Sci. Technol.* **2007**, *18*, 117−131.

(17) Guilminot, E.; Gavillon, R.; Chatenet, M.; Berthon-Fabry, A.; Rigacci, A.; Budtova, T. New Nanostructured Carbons Based on Porous Cellulose: Elaboration, Pyrolysis and Use as Platinum Nanoparticles Substrate for Oxygen Reduction Electrocatalysis. *J. Power Sources* **2008**, *185*, 717−726.

(18) Rooke, J.; Passos, C. M.; Chatenet, M.; Sescousse, R.; Budtova, T.; Berthon-Fabry, S.; Mosdale, R.; Maillard, F. Synthesis and Properties of Platinum Nanocatalyst Supported on Cellulose-Based Carbon Aerogel for Applications in PEMFCs. *J. Electrochem. Soc.* **2011**, *158*, B779−B789.

(19) Seo, J. A.; Kim, J. C.; Koh, J. K.; Ahn, S. H.; Kim, J. H. Preparation and Characterization of Crosslinked Cellulose/Sulfosuccinic Acid Membranes as Proton Conducting Electrolytes. *Ionics* **2009**, *15*, 555−560.

(20) Gama, M.; Gatenholm, P.; Klemm, D. *Bacterial Nanocellulose: A Sophisticated Multifunctional Material*; CRC Press: Boca Raton, FL, 2012.

(21) Klemm, D.; Schumann, D.; Udhardt, U.; Marsch, S. Bacterial Synthesized Cellulose -Artificial Blood Vessels for Microsurgery. *Prog. Polym. Sci.* **2001**, *26*, 1561−1603.

(22) Czaja, W.; Krystynowicz, A.; Bielecki, S.; Brown, R. M. Microbial Cellulose−The Natural Power to Heal Wounds. *Biomaterials* **2006**, *27*, 145−151.

(23) Trovatti, E.; Silva, N. H. C. S.; Duarte, I. F.; Rosado, C. F.; Almeida, I. F.; Costa, P.; Freire, C. S. R.; Silvestre, A. J. D.; Neto, C. P. Biocellulose Membranes as Supports for Dermal Release of Lidocaine. *Biomacromolecules* **2011**, *12*, 4162−4168.

(24) Iguchi, M. S.; Mitsuhashi, S.; Ichimura, K.; Nishi, Y.; Uryu, M.; Yamanaka, S.; Watanabe, K. Bacterial Cellulose-Containing Molding Material Having High Dynamic Strength. U.S. Patent 4742164, 1988.

(25) Shah, J.; Brown, R. M. Towards Electronic Paper Displays Made from Microbial Cellulose. *Appl. Microbiol. Biotechnol.* **2005**, *66*, 352−355.

(26) Trovatti, E.; Oliveira, L.; Freire, C. S. R.; Silvestre, A. J. D.; Neto, C. P.; Cruz Pinto, J. J. C.; Gandini, A. Novel Bacterial Cellulose−Acrylic Resin Nanocomposites. *Compos. Sci. Technol.* **2010**, *70*, 1148−1153.

(27) Tomé, L. C.; Pinto, R. J. B.; Trovatti, E.; Freire, C. S. R.; Silvestre, A. J. D.; Neto, C. P.; Gandini, A. Transparent Bionanocomposites with Improved Properties Prepared from Acetylated Bacterial Cellulose and Poly(lactic acid) through a Simple Approach. *Green Chem.* **2011**, *13*, 419−427.

(28) Evans, B. R.; O'Neill, H. M.; Malyvanh, V. P.; Lee, I.; Woodward, J. Palladium-Bacterial Cellulose Membranes for Fuel Cells. *Biosens. Bioelectron.* **2003**, *18*, 917−923.

(29) Yanga, J.; Suna, D.; Li, J.; Yang, X.; Yu, J.; Hao, Q.; Liu, W.; Liu, J.; Zou, Z.; Gu, J. In Situ Deposition of Platinum Nanoparticles on Bacterial Cellulose Membranes and Evaluation of PEM Fuel Cell Performance. *Electrochim. Acta* **2009**, *54*, 6300−6305.

(30) Wainright, J. S.; Wang, J. T.; Weng, D.; Savinell, R. F.; Litt, M. Acid-Doped Polybenzimidazoles: A New Polymer Electrolyte. *J. Electrochem. Soc.* **1995**, *142*, L121−L123.

(31) Gaopeng, J.; Jinli, Q.; Feng, H. Application of Phosphoric Acid and Phytic Acid-Doped Bacterial Cellulose as Novel Proton-Conducting Membranes to PEMFC. *Int. J. Hydrogen Energy* **2012**, *37*, 9182−9192.

(32) Lin, C. W.; Liang, S. S.; Chen, S. W.; Lai, J. T. Sorption and Transport Properties of 2-Acrylamido-2-methyl-1-propanesulfonic Acid-Grafted Bacterial Cellulose Membranes for Fuel Cell Application. *J. Power Sources* **2013**, *232*, 297−305.

(33) Figueiredo, F. M. L.; Gadim, T. O.; Figueiredo, A. G. P. R.; Rosero-Navarro, N. C.; Gamelas, J. A. F.; Freire, C. S. R.; Silvestre, A. J. D. *Bacterial Cellulose-Polystyrene Sulfonic Acid Nanocomposite Proton Conductors*, 19th International Conference on Solid State Ionics, Kyoto (Japan) 2013 (invited lecture).

(34) Ding, J.; Chuy, C.; Holdcroft, S. A Self-organized Network of Nanochannels Enhances Ion Conductivity through Polymer Films. *Chem. Mater.* **2001**, *13*, 2231−2233.

(35) Savadogo, O. Emerging Membranes for Electrochemical Systems: (I) Solid Polymer Electrolyte Membranes for Fuel Cell Systems. *J. New Mater. Electrochem. Syst.* **1998**, *1*, 47−66.

(36) Lehtinen, T.; Sundholm, G.; Holmberg, S.; Sundholm, F.; Björnbom, P.; Bursell, M. Electrochemical Characterization of PVDF-Based Proton Conducting Membranes for Fuel Cells. *Electrochim. Acta* **1998**, *43*, 1881−1890.

(37) Büchi, E. N.; Gupta, B.; Haas, O.; Scherer, G. G. Study of Radiation-Grafted FEP-g-Polystyrene Membranes as Polymer Electrolytes in Fuel Cells. *Electrochim. Acta* **1995**, *40*, 345−353.

(38) Martins, C. R.; Ruggeri, G.; Paoli, M. A. D. Synthesis in Pilot Plant Scale and Physical Properties of Sulfonated Polystyrene. *J. Braz. Chem. Soc.* **2003**, *14*, 797−802.

(39) Yu, J.; Yi, B.; Xing, D.; Liu, F.; Shao, Z.; Fu, Y.; Zhang, H. Degradation Mechanism of Polystyrene Sulfonic Acid Membrane and Application of its Composite Membranes in Fuel Cells. *Phys. Chem. Chem. Phys.* **2003**, *5*, 611−615.

(40) Panwar, V.; Cha, K.; Park, J.-O.; Park, S. High Actuation Response of PVDF/PVP/PSSA Based Ionic Polymer Metal Composites Actuator. *Sens. Actuators, B* **2012**, *161*, 460−470.

(41) Pinto, N. J.; Rivera, D.; Melendez, A.; Ramos, I.; Limb, J. H.; Johnson, A. T. C. Electrical Response of Electrospun PEDOT-PSSA Nanofibers to Organic and Inorganic Gases. *Sens. Actuators, B* **2011**, *156*, 849−853.

(42) Lacerda, P. S. S.; Barros-Timmons, A. M. M. V.; Freire, C. S. R.; Silvestre, A. J. D.; Neto, C. P. Nanostructured Composites Obtained by ATRP Sleeving of Bacterial Cellulose Nanofibers with Acrylate Polymers. *Biomacromolecules* **2013**, *14*, 2063−2073.

(43) E.I. du Pont de Nemours and Company, DuPont Fuel Cells, DuPont Nafion PFSA Membranes N115, N117, N1110. Technical Brochure DFC101.0209.

(44) Solvay Specialty Polymers, Aquivion PFSA Technical Data, February 2013.

(45) Nishiyama, Y.; Sugiyama, J.; Chanzy, H.; Langan, P. Crystal Structure and Hydrogen Bonding System in Cellulose Iα from Synchrotron X-ray and Neutron Fiber Diffraction. *J. Am. Chem. Soc.* **2003**, *125*, 14300−14306.

(46) Garvey, C. J.; Parker, I. H.; Simon, G. P. On the Interpretation of X-Ray Diffraction Powder Patterns in Terms of the Nanostructure of Cellulose I Fibres. *Macromol. Chem. Phys.* **2005**, *206*, 1568−1575.

(47) Wu, J.; Zheng, Y.; Yang, Z.; Cui, Q.; Wang, Q.; Gao, S.; Ding, X. Chemical Modifications and Characteristic Changes in Bacterial Cellulose Treated with Different Media. *J. Polym. Res.* **2012**, *19*, 9945.

(48) Hardy, B. J.; Sarko, A. Molecular Dynamics Simulations and Diffraction-Based Analysis of the Native Cellulose Fibre: Structural Modelling of the I-A and I-B Phases and their Interconversion. *Polymer* **1996**, *37*, 1833−1839.

(49) Meshitsuka, G. I.; Isogai, A. In *Chemical Modification of Lignocellulosic Materials*; Hon, D. N.-S., Ed.; CRC Press: New York, 1996; Chapter 2, pp 11−34.

(50) Ningping, C.; Hong, L. A Study on Polypyrrole-Coated Polystyrene Sulfonic Acid Microspheres−A Proton Electrolyte. *Eur. Polym. J.* **2001**, *37*, 1027−1035.

(51) Amarasekara, A. S.; Wiredu, B. Aryl Sulfonic Acid Catalyzed Hydrolysis of Cellulose in Water. *Appl. Catal. A* **2012**, *417−418*, 259−262.

(52) Roman, M.; Winter, W. T. Effect of Sulfate Groups from Sulfuric Acid Hydrolysis on the Thermal Degradation Behavior of Bacterial Cellulose. *Biomacromolecules* **2004**, *5*, 1671−1677.

(53) Suganuma, S.; Nakajima, K.; Kitano, M.; Yamaguchi, D.; Kato, H.; Hayashi, S.; Hara, M. Hydrolysis of Cellulose by Amorphous Carbon Bearing SO_3H, COOH, and OH Groups. *J. Am. Chem. Soc.* **2008**, *130*, 12787−12793.

(54) Tamaki, R.; Chujo, Y. Synthesis of Polystyrene and Silica Gel Polymer Hybrids Utilizing Ionic Interactions. *Chem. Mater.* **1999**, *11*, 1719−1726.

(55) Yadav, R.; Fedkiw, P. S. Analysis of EIS Technique and Nafion 117 Conductivity as a Function of Temperature and Relative Humidity. *J. Electrochem. Soc.* **2012**, *159*, B340−B346.

(56) Maréchal, M.; Souquet, J.-L.; Guindet, J.; Sanchez, J.-Y. Solvation of Sulphonic Acid Groups in Nafion® Membranes from Accurate Conductivity Measurements. *Electrochem. Commun.* **2007**, *9*, 1023−1028.

(57) Alberti, G.; Casciola, M.; Massinelli, L.; Bauer, B. Polymeric Proton Conducting Membranes for Medium Temperature Fuel Cells (110−160 °C). *J. Membr. Sci.* **2001**, *185*, 73−81.

(58) Rosero-Navarro, N. C.; Domingues, E. M.; Sousa, N.; Ferreira, P.; Figueiredo, F. M. L. Meso-Structured Organosilicas as Fillers for Nafion® Membranes. *Solid State Ionics* **2014**, DOI: 10.1016/j.ssi.2013.09.058.

(59) Shen, Y.; Qiu, X.; Shen, J.; Xi, J.; Zhu, W. PVDF-g-PSSA and Al_2O_3 Composite Proton Exchange Membranes. *J. Power Sources* **2006**, *161*, 54−60.

(60) Aslan, A.; Şen, Ü.; Bozkurt, A. Preparation, Properties, and Characterization of Polymer Electrolyte Membranes Based on Poly(1-vinyl-1,2,4 triazole) and Poly(styrene sulfonic acid). *J. Electrochem. Soc.* **2009**, *156*, B1112−B1116.

(61) Clochard, M.-C.; Berthelot, T.; Baudina, C.; Betza, N.; Balanzat, E.; Gébel, G.; Morin, A. Ion Track Grafting: A Way of Producing Low-Cost and Highly Proton Conductive Membranes for Fuel Cell Applications. *J. Power Sources* **2010**, *195*, 223−231.

(62) Eikerling, M.; Kornyshev, A. A. Proton Transfer in a Single Pore of a Polymer Electrolyte Membrane. *J. Electroanal. Chem.* **2001**, *502*, 1−14.

(63) Vayenas, C. G.; Tsampas, M. N.; Katsaounis, A. First Principles Analytical Prediction of the Conductivity of Nafion Membranes. *Electrochim. Acta* **2007**, *52*, 2244−2256.

(64) Vargas, M. A.; Vargas, R. A.; Mellander, B.-E. New Proton Conducting Membranes Based on $PVAL/H_3PO_2/H_2O$. *Electrochim. Acta* **1999**, *44*, 4227−4232.

(65) Schuster, M. F. H.; Meyer, H. W.; Schuster, M.; Kreuer, K. D. Toward a New Type of Anhydrous Organic Proton Conductor Based on Immobilized Imidazole. *Chem. Mater.* **2004**, *16*, 329−337.

(66) Depre, L.; Ingram, M.; Poinsignon, C.; Popall, M. Proton Conducting Sulfon/Sulfonamide Functionalized Materials based on Inorganic−Organic Matrices. *Electrochim. Acta* **2000**, *45*, 1377−1383.

(67) Metatla, N.; Soldera, A. The Vogel−Fulcher−Tamman Equation Investigated by Atomistic Simulation with Regard to the Adam−Gibbs Model. *Macromolecules* **2007**, *40*, 9680−9685.

(68) Carreira, P.; Mendes, J. A. S.; Trovatti, E.; Serafim, L. S.; Freire, C. S. R.; Silvestre, A. J. D.; Neto, C. P. Utilization of Residues from Agro-Forest Industries in the Production of High Value Bacterial Cellulose. *Bioresour. Technol.* **2011**, *102*, 7354−7360.

(69) Hestrin, S.; Schramm, M. Synthesis of Cellulose by Acetobacter Xylinum. 2. Preparation of Freeze-Dried Cells Capable of Polymerizing Glucose to Cellulose. *Biochem. J.* **1954**, *58*, 345−352.